Catalysis Today 418 (2023) 114145

Contents lists available at ScienceDirect

Catalysis Today

journal homepage: www.elsevier.com/locate/cattod

Au/TiO_2 coatings for photocatalytic reduction of 4-nitrophenol to 4-aminophenol with green light

Joseph W. Gregory [a], Yuyan Gong [a], Yisong Han [b], Steven Huband [b], Richard I. Walton [c], Volker Hessel [a,d], Evgeny V. Rebrov [a,e,*]

[a] School of Engineering, University of Warwick, Coventry CV4 7AL, UK
[b] Department of Physics, University of Warwick, Coventry CV4 7AL, UK
[c] Department of Chemistry, University of Warwick, Coventry CV4 7AL, UK
[d] School of Chemical Engineering, The University of Adelaide, Adelaide, SA 5005, Australia
[e] Department of Chemical Engineering and Chemistry, Eindhoven University of Technology, P.O. Box 513, 5600 MB Eindhoven, the Netherlands

ARTICLE INFO

Keywords:
Gold nanoparticle
Photocatalysis
Green light
Thin film
Au/TiO_2
Combustion-evaporation
Langmuir-Hinshelwood kinetics

ABSTRACT

Au/TiO_2 catalytic coatings have been developed onto the inner surface of a quartz tube for photocatalytic applications. Gold nanoparticles with diameter 3–5 nm were synthesised using the citrate method, with sodium borohydride as a reducing agent. The nanoparticles were characterised by UV–vis spectroscopy, small angle X-ray scattering (SAXS), dynamic light scattering (DLS), and transmission electron microscopy (TEM). The photocatalytic activity of gold nanoparticles and Au/TiO_2 catalytic coatings was studied in the reduction of 4-nitrophenol (4-NP) with green LEDs. The reaction rate follows Langmuir-Hinshelwood kinetics and increases with the light intensity until a plateau at 3 mW cm^{-2}. The photocatalytic activity of gold nanoparticles was fully preserved in the Au/TiO_2 coatings.

1. Introduction

Catalysts used in plasma-assisted catalytic processes are mostly "thermal" catalysts that are used under non-plasma conditions and at higher temperatures for similar reactions [1]. While several studies have reported the promotion effect in the presence of a conventional catalyst, this is often observed at higher temperatures, while non-thermal plasma usually requires ambient temperature and pressure. To make operation at room temperature possible, a combination of semiconductors with a photocatalytic metal is a promising strategy. Surface charges can be generated and transferred to the semiconductor under external irradiation [2]. In many cases, photocatalysis is considered to be a proxy for non-thermal plasma, as the catalysts with high photocatalytic activity remain active under plasma-catalysis conditions [3,4].

The choice of gold nanoparticles as the metal catalyst is related to the favourable chemical and physical properties of this noble metal. In particular, gold is an efficient catalyst for hydrogenation/dehydrogenation [5–7] and oxidation reactions [8]. Although the overall rate of reduction over gold nanoparticles is lower when compared to the reaction rates achievable with Pd and Pt catalysts, the application of gold catalysts remains attractive due to its photocatalytic properties and higher selectivity [9]. Beyond thermal catalysis, nanoscale gold facilitates photocatalytic processes in the ultraviolet (UV) and visible range, even for large band gap semiconductor supports [10]. Gold nanoparticles absorb light in the visible range and the resulting electron density oscillation is used for photocatalysis [11].

Titania is a low-cost, nontoxic, and stable material, making it an ideal support for gold-based catalysts [12]. It has been extensively studied in photocatalysis, mainly in the area of pollutant abatement [13]. On semiconductors, like titania, light absorption by gold generates localised surface plasmons (oscillations of electron density). The possibility to tailor absorption wavelengths and carrier transport properties by changing the nanoparticle size and by doping, in combination with the high surface-to-volume ratio of titania thin films, is promising for applications in photocatalysis and non-thermal plasma catalysis [14,15].

Photocatalytic reduction of CO_2 into hydrocarbon-based fuels over Au/TiO_2 catalysts is a promising technique in the development of artificial photosynthesis strategies [16,17]. There are also examples of N_2 activation over gold nanoparticles [18]. It is generally agreed that the type of support material and the gold–support interfacial sites generated

* Corresponding author.
E-mail addresses: E.Rebrov@warwick.ac.uk, E.Rebrov@tue.nl (E.V. Rebrov).

https://doi.org/10.1016/j.cattod.2023.114145
Received 14 January 2023; Received in revised form 20 March 2023; Accepted 1 April 2023
Available online 5 April 2023

play a crucial role in determining the catalytic behaviour of supported gold nanoparticles [19,20].

Among the various methods developed for preparing supported gold nanoparticles, deposition–precipitation (DP) is one of the main methods. Haruta et al. first succeeded in making active gold catalysts using this method [21]. During DP synthesis, a key parameter is the surface charge state of titania, which depends on the pH value, meaning that the isoelectric point (IEP) of titania (in the range 4.5–6.3) must be considered [22]. In this method, the nature of the gold colloids depends on the pH value, the ionic strength of the solution, and the reaction temperature. Also, at pH values above 9 the gold loading onto the support is limited by the increasing solubility of the gold hydroxide species [23]. To ensure most of the gold is located within the mesoporous framework of the support, it is possible to perform a one-pot synthesis of the mesoporous support and gold nanoparticles [5]. This method allows the achievement of 100% uptake of colloidal gold nanoparticles into the thin films. Uniform 4–5 nm gold nanoparticles with up to 3 wt% loading were prepared within the titania pores by this method. However, in order to control gold particle size in a wider range, a two-step synthesis is usually required. In the first step, titania thin film synthesis is performed by an evaporation induced self-assembly (EISA) method [24–26], followed by an gold deposition step. While the classical EISA method allows control of the morphology and porosity of thin films over a wide range of conditions, the main limitation of the method remains a low coating thickness which requires multiple deposition runs to obtain the desirable thickness in the range of about 10–15 μm [27]. In contrast, the combustion-evaporation method can obtain a coating thickness above a few microns in a single deposition run [28]. A similar approach using a modification of the original method was subsequently reported by Svetlov et al. [29]. They added a non-reacting gas, altering its flow rate to better control boiling conditions inside the tube. The morphology and thickness of the titania coatings is controlled by boiling conditions and the modified method resulted in more uniform coatings. This makes it possible to prepare gold catalysts on "engineered" nanostructured titania thin films for photocatalytic applications.

In this study, we design and carry out a novel method for photocatalytic reactions, whilst showing that understanding derived from simpler experiments can be applied to work carried out in thin film-coated tubes. The application of Au/TiO_2 catalysts and initial Au(0) nanoparticles in the reduction of 4-nitrophenol (4-NP) to 4-aminophenol (4-AP) (a model reaction often used for determining kinetic and thermodynamic parameters [30–32]) provides the groundwork for this research, and the quantification of the effect of the optical power density on the Langmuir-Hinshelwood kinetics of the reaction gives insight into the effectiveness of the system.

2. Experimental

2.1. Catalyst synthesis

Gold nanoparticles were synthesised by mixing 10 mL of an aqueous mixture of $HAuCl_4$ (0.50 mM, 99.99 wt%, VWR) and sodium citrate (0.50 mM, 99.0 wt%, Sigma-Aldrich) with ice-cold aqueous sodium borohydride (10 mL, 6.0 mM, 97 wt%, Scientific Laboratory Supplies Ltd) following the method used by Jana et al. [33]. The suspensions were kept in the dark at room temperature for 96 h before being stored in the dark at 4 °C. These nanoparticles were subsequently used as-synthesised both for catalytic testing and to produce coatings.

A TiO_2 coating was produced on the internal surface of a quartz tube using our previous method [29]. Briefly, a quartz tube (ID: 3 mm, OD: 5 mm) was cleaned with a 4 M aqueous NaOH solution and then washed with water. Polyvinylpyrrolidone (PVP) (3.0 g, MW: 40,000), P25 TiO_2 (3.0 g) and methanol (40 mL) were mixed for 30 min to produce the coating solution. The coating solution was fed into the quartz tube from its bottom end using a syringe pump together with the compressed air. The quartz tube was fed at a rate 1.1 mm s^{-1} into a vertical furnace maintained at 175 °C. Finally, the coated quartz tube was calcined for 2 h at 450 °C with a heating ramp of 1 °C min^{-1}. The Au nanoparticles were deposited from a suspension of colloidal nanoparticles (0.5 mL). The tube was dried at 90 °C and then calcined at 450 °C for 2 h with a heating rate of 1 K min^{-1}. The Au deposition process is shown in Fig. 1.

2.2. Catalyst characterisation

The phase composition was determined with X-ray diffraction (XRD) using a Panalytical X'Pert Pro MPD diffractometer with CuKα_1 radiation over the range $2\theta = 20–70°$ at a scanning rate of 0.06° min^{-1}. The morphology was studied with scanning electron microscopy (SEM) using a Zeiss SUPRA 55VP FEGSEM apparatus. UV–vis spectroscopy was conducted using a Shimadzu UV-2600 spectrophotometer in the range 300–700 nm; OriginPro software was used for peak fitting of gold nanoparticle spectra, using an asymmetric double sigmoidal function. Small angle X-ray scattering (SAXS) was used to characterise particle size and measurements were made using a Xenocs Xeuss 2.0 instrument equipped with a micro-focus Cu Kα source collimated with scatterless slits. The samples were mounted in 1 mm thick borosilicate glass capillaries and the scattering was collected at room temperature for 4 h. The scattering of the gold nanoparticles was modelled using SasView v5 software.

Dynamic light scattering (DLS) was conducted using an Anton Paar Litesizer 500 (0.3–2000 nm) with the sample suspended in deionised water for the calculation of the intensity weighted diameter. Transmission electron microscopy (TEM) was conducted using a JEOL JEM-2100Plus (200 kV). Bright field TEM images were taken using a JEOL ARM200F (200 kV). For average particle sizes, a sample of a minimum of 100 particles was used. For non-spherical particles, the diameter was calculated by Eq. 1.

$$d = \frac{d_1 + d_2}{2}, \tag{1}$$

where d_1 is the large diameter and d_2 is the small diameter [34].

2.3. Photocatalytic testing

The reduction of 4-NP to 4-AP was chosen as a test reaction (Scheme 1). For the testing of the gold nanoparticles in suspension, a reaction mixture consisting of an aqueous solution (39.4 mL) of 4-NP (0.11 mol L^{-1}, 99 wt%, Alfa Aesar), and sodium borohydride (3.0 mmol L^{-1}) was irradiated by green LEDs at a constant temperature of 2 °C. The reaction was initiated by the addition of as-synthesised Au catalyst suspension (0.6 mL). The maximum optical power density was 6.4 mW cm^{-2} and the optical emission spectrum of the LED light source is shown in Fig. S1. Samples were taken at desired time intervals and immediately analysed using UV–vis spectroscopy over the range 300–700 nm. The 4-NP peak at 400 nm was fitted using an asymmetric double sigmoidal function, while all other peaks were fitted using a Gaussian function.

The Au/TiO_2 coatings were tested with a mixture (0.6 mL) of 4-NP (2.2 mmol L^{-1}) and sodium borohydride (30 mmol L^{-1}). The samples of 0.05 mL were extracted and made up to 1.0 mL with water for UV–vis analysis.

Sodium borohydride was used in excess in both sets of photocatalytic testing experiments so that it can be treated as having zero order kinetics. The Langmuir-Hinshelwood equation [35,36] provided the best fit in comparison to zero and first order plots for experimental data (Eq. 2).

$$(c_0 - c_t) + \frac{1}{K}\ln\frac{c_0}{c_t} = -k_{LH}t, \tag{2}$$

where t is time, c_0 is initial concentration, c_t is concentration at time t, K is the equilibrium constant, and k_{LH} is the kinetic constant. A first order

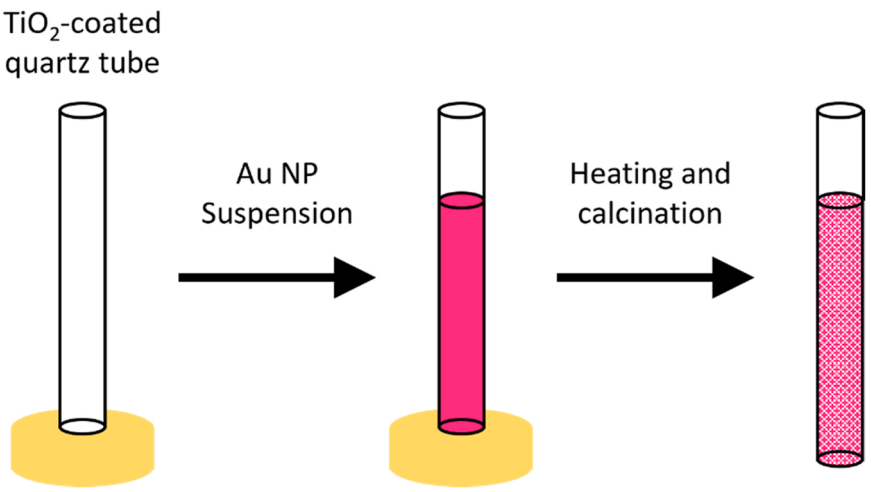

Fig. 1. A representation of the Au deposition on the internal surface of a TiO_2-coated quartz tube.

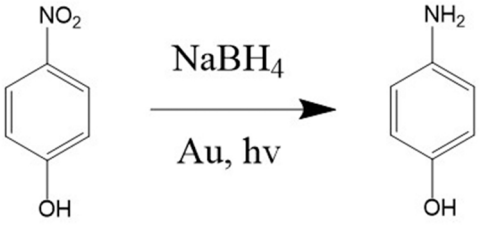

Scheme 1. The reduction of 4-NP to produce 4-AP.

rate constant (k_1, Eq. 3) was also calculated for a proper comparison with literature data.

$$\ln(c_t) = -k_1 t + \ln(c_0) \quad (3)$$

3. Results & discussion

3.1. Characterisation

SAXS was used for particle size and polydispersity characterisation. The particles were modelled as spheres with the radius given by a log-normal number distribution. The scattered intensity from a sphere was fitted by Eq. 4 (see Fig. 2).

$$I(q) = \frac{V_f}{V}.\left[3V(\Delta\rho).\frac{\sin(qr) - qr\cos(qr)}{(qr)^3}\right]^2 + background, \quad (4)$$

where q is the scattering vector, $q = \frac{4\pi\sin\theta}{\lambda}$, V_f is the volume fraction, V is the volume and $\Delta\rho$ is the scattering length density difference between the particles and solvent [37]. A mean particle size of 3.2 ± 1.3 nm was obtained.

DLS results for particle size and polydispersity gave a diameter of 5.3 ± 0.8 nm (Fig. 3, Fig. S2). It is well documented that DLS calculates the diameter of the particles including the ligands (in this instance citrate), which is the likely explanation of the particle size given by this technique being larger than that given by SAXS [38–40].

TEM imaging was also used to confirm the mean particle diameter and a value of 5.1 ± 1.0 nm was obtained from image analysis (Fig. 4a). A reason for the discrepancy between the diameters given by TEM (Fig. 4b) and SAXS (Fig. 2) is likely that SAXS averages over all particles, whereas the value determined by TEM averages over all particles which can be observed from the images, meaning that it is possible for smaller particles to be excluded if they overlap with larger particles.

The image of the Au/TiO_2 coating (Fig. 4c) shows agglomeration. The mean diameter of gold nanoparticles in the coating was 24.5 ± 18.2 nm (Fig. 4d). This may not be an accurate assessment of the particle size, as there is a change in particle shape after deposition onto the titania coating. Many of the agglomerates are elongated or of irregular shape, and there are still many smaller particles which have not been significantly affected. However, it does clearly illustrate a significant change both in particle size and in particle size distribution

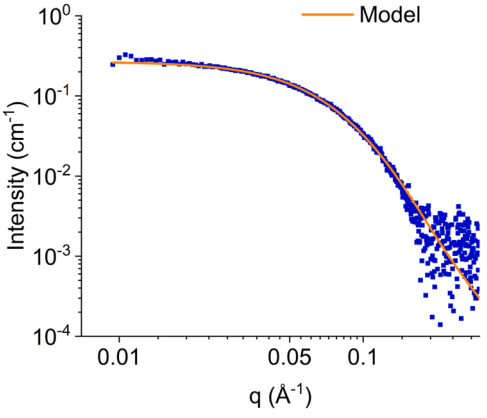

Fig. 2. The SAXS pattern of the gold nanoparticles. The blue points show the experimental data and the orange curve shows the curve fitted by Eq.4.

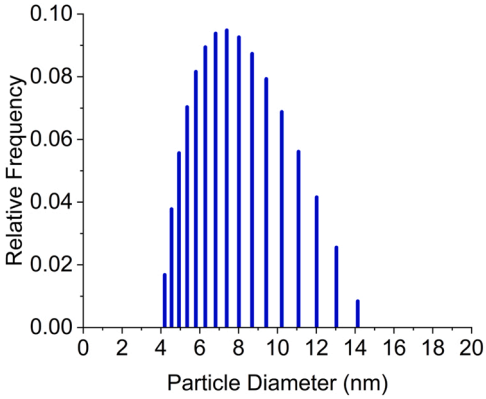

Fig. 3. The particle size distribution determined by DLS.

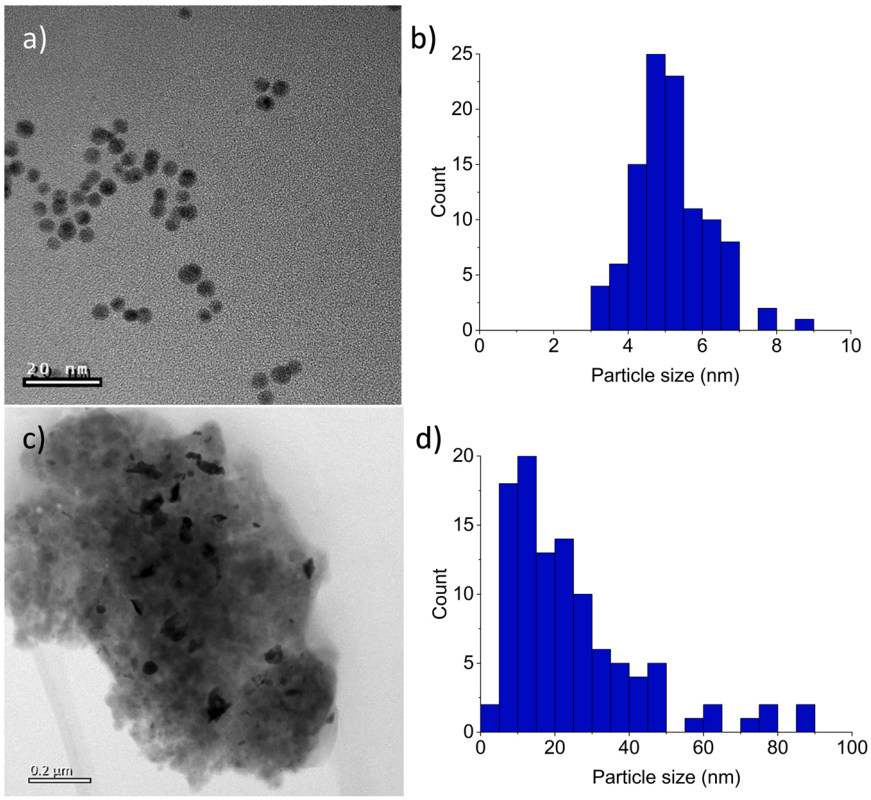

Fig. 4. a) A TEM image of the synthesised gold nanoparticles in suspension, b) a histogram of particle sizes for the gold nanoparticle suspension, c) a bright field TEM image of the Au/TiO_2 coating from the tubes, and d) a histogram of particle sizes for the Au/TiO_2 coating from the tubes.

compared to the unsupported catalyst.

The UV–vis spectrum of the gold nanoparticle suspension (Fig. 5a) shows an absorption peak with a maximum at 514 nm. Typically, the UV−vis spectrum of spherical nonaggregated gold nanoparticles is represented by a band around 520 nm, due to the SPR, plus an absorption edge at shorter wavelengths due to interband transitions of d-band electrons [41].

A comparison of the UV–vis spectrum with literature suggests that the mean gold nanoparticle size is approximately 5 nm (Fig. 6), which was confirmed by TEM. For smaller gold nanoparticle sizes (2 −4 nm), quantum size effects influence the shape and position of the surface plasmon resonance (SPR) band. Additionally, the behaviour of the d-band electrons depends on surface coating and size [42]. Since the SPR gives rise to an absorption spectrum which depends on the size, shape, and aggregation of gold nanoparticles, UV−vis spectroscopy is a useful method which allows for the estimation of gold nanoparticle size and concentration. However, in many cases this approach gives unreliable results because the position of the plasmon resonance is affected by multiple factors, like environment dielectric properties [43], physical or chemical interactions on particles surface [44] and aggregation [45]. Therefore, additional independent methods of analysis such as SAXS and TEM are still necessary.

Incorporation of gold nanoparticles in a titania coating shifts the position of the peak to 560 nm (Fig. 5b), and absorption by the titania can be seen in the 300–400 nm range. The increase in wavelength upon coating could result from agglomeration of nanoparticles upon heating

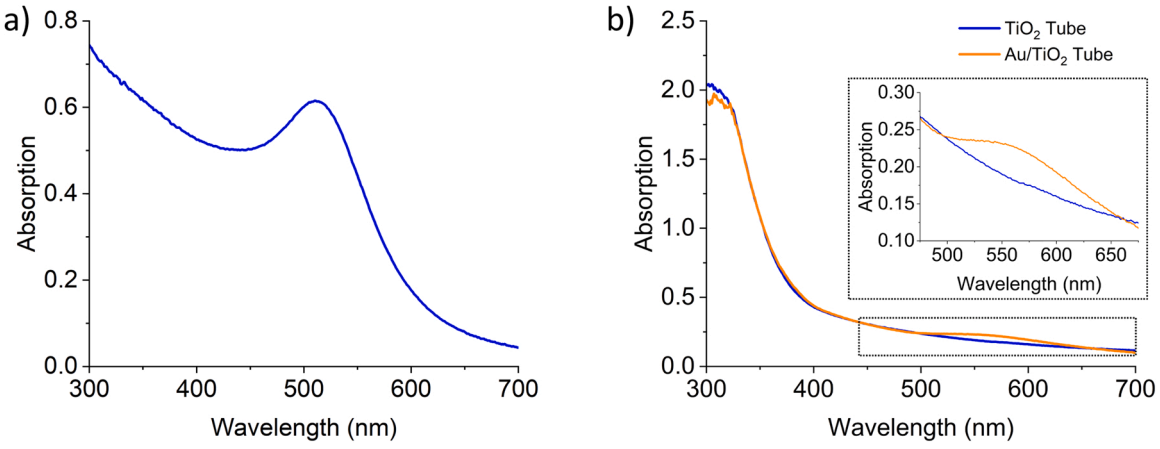

Fig. 5. a) The UV–vis spectrum of the synthesised gold nanoparticle suspension b) The UV–vis spectra of the TiO_2 coated tube before and after coating with gold nanoparticles with insert enlarged in the gold nanoparticle absorption region.

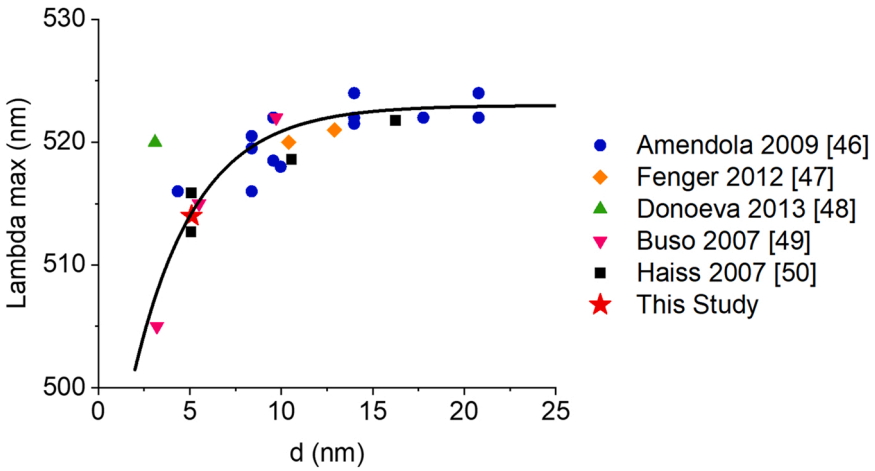

Fig. 6. A comparison of the correlation between particle size (d) and lambda max from the gold nanoparticles synthesised in this study with literature values for spherical gold nanoparticles in suspension [46–50]. A fit is shown as a guide to the trend of changing lambda max over this range of diameters.

rather than from interaction between the gold nanoparticles and the TiO_2 support affecting optical properties.

The Au/TiO_2 coating consists of a mixture of anatase and rutile in approximately equal proportion (Fig. 7). Among TiO_2 polymorphs, anatase-phase TiO_2 is believed to have a superior photocatalytic activity to pure rutile and brookite [51,52]. In the synthesis of the coated tubes, calcination resulting in strong metal support interactions whilst preserving high photocatalytic ability was essential. TiO_2 becomes phase-pure rutile at approximately 600 °C [53], which was a factor considered when deciding upon a calcination temperature, however the calcination gave rise to the transformation of some anatase to rutile, resulting in a higher rutile proportion than P25 titania (25%).

An SEM image of the TiO_2 thin film shows that the average coating thickness is 2 μm (Fig. 8).

3.2. Photocatalytic testing

A significant proportion of 4-NP had reacted within 30 min at the higher optical power densities used (Fig. S2). The 4-NP peak at 400 nm decreases with time, whilst the 4-AP peak increases with time. The selectivity towards 4-AP was 60%.

The reaction kinetics fitted well to the Langmuir-Hinshelwood (LH) model (Eq. 2). This was deemed to be the most appropriate model, with the zero order and first order models providing worse fits. Therefore, the kinetic and equilibrium constants were obtained from the fitting of kinetic data using LH model (Fig. 9). A blank experiment without the Au catalyst showed zero conversion. However, some minor conversion of 4-NP was observed in the absence of external irradiation, suggesting a small thermal catalytic contribution for the reaction over the Au catalyst.

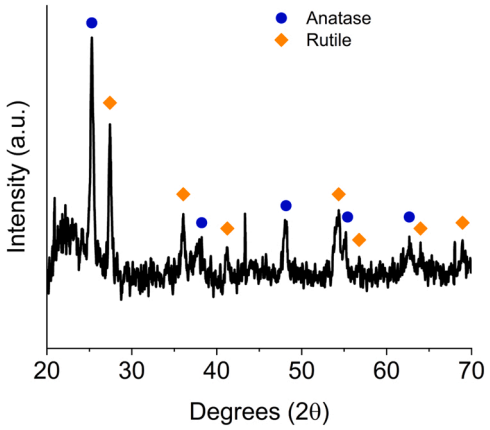

Fig. 7. XRD pattern of TiO_2 coated tube with peaks representing different phases marked. The TiO_2 in the coating is clearly comprised of a mixture of anatase and rutile.

The kinetic data obtained show an optical saturation regime, whereby an increase in optical power density increases the rate of reaction up to a saturation intensity, above which the rate plateaus (Fig. 10). However, below an optical power density of 3 mW cm^{-2}, the LH constant increases with increasing the green light intensity. The saturation happens at a significantly lower optical power density than in other studies over Au catalysts [54,55]. Other studies have generally calculated a first order rate constant (k_1), rather than a LH rate constant and, as such, k_1 was calculated in order to compare the results of this study with literature values. k_1 was obtained by Eq. 3. A catalyst normalised constant, k_1' (Eq. 5), was used for a more equitable comparison.

$$k_1' = k_1 / c_{Au}, \tag{5}$$

where c_{Au} is the concentration of gold in the reaction mixture. The results from this study show a similar k_1' to those reported in the literature (Table 1) [56–59]. It must be considered that the literature studies were carried out at room temperature, whereas this study was carried out at 2 °C to reduce the contribution from the thermal reaction, and, as such, a slower rate would be expected. It is, however, notable that the rate observed is comparable with many literature data.

The values found for K are consistent ($9.2 \times 10^3 \pm 0.7 \times 10^3$ dm^3 mol^{-1}), indicating that the reaction mechanism was the same at each optical power density as well as when the experiment was conducted in the dark (Table S1).

The conversion over Au/TiO_2 was 60.1% after 30 min under irradiation with green light, mirroring the effect by Au nanoparticles in suspension. Fig. 11 shows that the conversion over Au/TiO_2 in the dark (44.5% conversion after 30 min) was greater than that over the TiO_2 support in the dark (22.3%), which demonstrated that the rate of thermal reaction was considerably higher over the Au/TiO_2 coatings.

The k_{LH} value of 4.6×10^{-5} min^{-1} was obtained over the Au/TiO_2 coatings under green light irradiation. When normalised for the Au concentration, it gives a value of 4.1×10^{-7} min^{-1} which is very close to the value obtained over the Au nanoparticles in suspension (4.0×10^{-7} min^{-1}). This shows that the properties of Au nanoparticles remain the same in suspension and after deposition on the titania thin films.

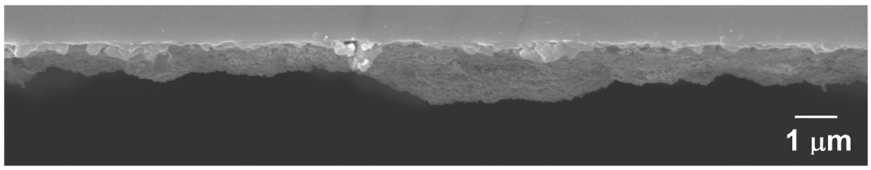

Fig. 8. An SEM image showing the TiO_2 thin film on the internal surface of a quartz tube.

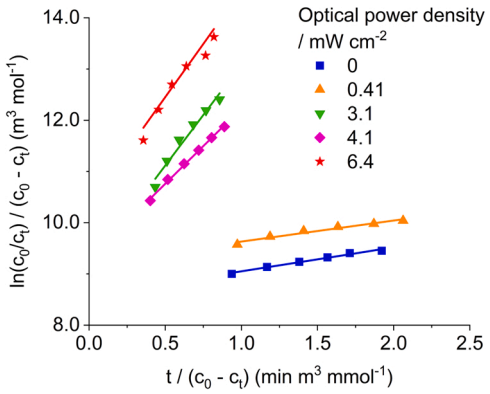

Fig. 9. A linear plot to determine K and k_{LH}, as described in the experimental section, from a reaction carried out under 6.4 mW cm^{-2} irradiation. Reactions were carried out at 2 °C using an aqueous solution of 4-NP (0.11 mol L^{-1}, 40 mL) and sodium borohydride (3.0 mmol L^{-1}) activated by gold nanoparticle suspension (0.6 mL) and irradiated by green LEDs. The emission spectrum is shown in Fig. S1.

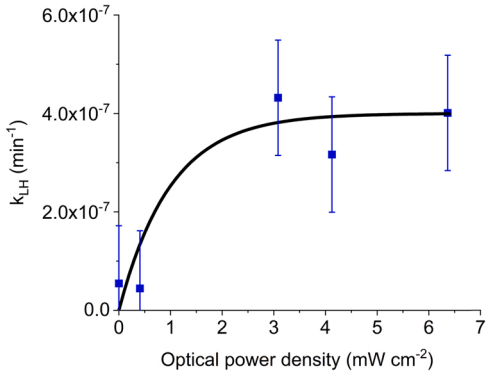

Fig. 10. A plot of the optical power density against the Langmuir-Hinshelwood rate constant (blue squares). A curve estimating the saturation regime is superimposed on the plot (black line).

Table 1
A comparison of first order rate constants for the reduction of 4-NP over gold nanoparticles in suspension obtained from this study with literature values for the same reaction with a version of the first order rate constant which has been normalised for gold concentration (k_1'). Diameters of the gold nanoparticles used for the catalysis (d) are provided along with the characterisation method.

k_1 (min^{-1})	k_1' ($dm^3\ mol^{-1}\ min^{-1}$)	d (nm)	Light Source	Ref
3.06×10^{-2}	Thin film	80 (SEM)	Laser (532 nm, 10 mW cm^{-2})	[56]
1.40×10^{-1}	1.53×10^{2}	13 (DLS)	None	[57]
8.40×10^{-1}	5.42×10^{4}	4 (TEM)	Unspecified	[58]
9.00×10^{-1}	3.00×10^{3}	20 (TEM)	Sunlight	[59]
1.30×10^{-2}	4.35×10^{3}	5 (TEM)	Green LEDs (6.4 mW cm^{-2})	This study

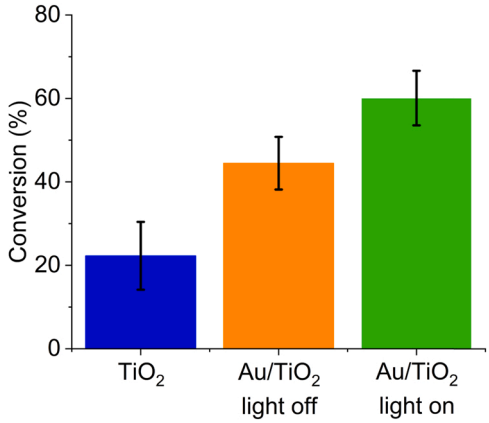

Fig. 11. A comparison of the 4-NP conversion after 30 min for reactions carried out in the TiO_2 coated tubes in the dark, the Au/TiO_2 coated tubes in the dark, and the Au/TiO_2 coated tubed under green light irradiation (6.4 mW cm^{-2}). All reactions shown in the bar chart were carried out at 2 °C using an aqueous solution of 4-NP (2.2 mmol L^{-1}) and sodium borohydride (30 mmol L^{-1}).

4. Conclusions

A uniform Au/TiO_2 coating with a thickness of 2 μm was successfully developed on the inner surface of quartz for application in photocatalysis under visible light. The catalytic films were tested in the photocatalytic reduction of 4-NP to 4-AP under illumination with green light. The reaction followed Langmuir-Hinshelwood kinetics, with adsorption being the rate-limiting step. The optical power density of saturation was relatively low (3 mW cm^{-2}) compared to literature values for similar catalysts. The photocatalytic activity of gold nanoparticles was fully preserved in the Au/TiO_2 coatings. The gold normalised rates were comparable with other studies demonstrating the absence of diffusion limitation in the catalytic coatings. This concept can be extended to photocatalytic applications in flow, with obvious applications in wastewater treatment, as well as potential utilisation in synthetic processes. The effect of combining UV with green light could be investigated to photoactivate the TiO_2 support. Given that photocatalysis is a proxy for non-thermal plasma conditions, the method has shown promise for plasma-catalytic applications under green light.

CRediT authorship contribution statement

Joseph W. Gregory: Experiment planning, conducting experiments, data analysis, writing, editing. **Yuyan Gong:** Experiments on TiO_2 coating, characterisation of TiO_2, writing. **Yisong Han:** Imaging methodology development, conducting bright field TEM, analysis of TEM images, contribution to Section 3.1. **Steven Huband:** Conducting SAXS, analysis of SAXS, contribution to Section 3.1. **Richard I. Walton:** Conception of experiments, interpretation of data, editing. **Volker Hessel:** Conception of study, editing. **Evgeny V. Rebrov**: Conception of study and experiments, interpretation of data, writing, final editing.

Declaration of Competing Interest

The authors declare that they have no known competing financial interests or personal relationships that could have appeared to influence the work reported in this paper.

Data availability

Data will be made available on request.

Acknowledgements

The authors acknowledge support from the ERC Synergy Grant "Surface-COnfined fast modulated Plasma for Process and Energy intensification" (SCOPE), from the European Commission, with Grant No. 810182. Some of the equipment was provided by the University of Warwick's Research Technology Platforms. We are particularly grateful for the assistance of Dr David Walker with XRD measurements. The contribution of Katie S. Pickering to the DLS characterisation is greatly appreciated.

Appendix A. Supporting information

Supplementary data associated with this article can be found in the online version at doi:10.1016/j.cattod.2023.114145.

References

[1] E.C. Neyts, K. Ostrikov, M.K. Sunkara, A. Bogaerts, Plasma catalysis: synergistic effects at the nanoscale, Chem. Rev. 115 (2015) 13408–13446, https://doi.org/10.1021/acs.chemrev.5b00362.
[2] G.V. Bianco, M.M. Giangregorio, P. Capezzuto, M. Losurdo, T.H. Kim, A.S. Brown, G. Bruno, Plasma-plasmonics synergy in the Ga-catalyzed growth of Si-nanowires, Mater. Sci. Eng. B Solid-State Mater. Adv. Technol. 177 (2012) 700–704, https://doi.org/10.1016/j.mseb.2011.09.030.
[3] L. Zhao, Y. Wang, L. Jin, M. Qin, X. Li, A. Wang, C. Song, Y. Hu, Decomposition of hydrogen sulfide in non-thermal plasma aided by supported CdS and ZnS semiconductors, Green. Chem. 15 (2013) 1509–1513, https://doi.org/10.1039/c3gc00092c.
[4] L. Zhao, Y. Wang, X. Li, A. Wang, C. Song, Y. Hu, Hydrogen production via decomposition of hydrogen sulfide by synergy of non-thermal plasma and semiconductor catalysis, Int. J. Hydrog. Energy 38 (2013) 14415–14423, https://doi.org/10.1016/j.ijhydene.2013.09.008.
[5] L.N. Protasova, E.V. Rebrov, H.E. Skelton, A.E.H. Wheatley, J.C. Schouten, A kinetic study of the liquid-phase hydrogenation of citral on Au/TiO_2 and Pt-Sn/TiO_2 thin films in capillary microreactors, Appl. Catal. A Gen. 399 (2011) 12–21, https://doi.org/10.1016/j.apcata.2011.03.021.
[6] P.G.N. Mertens, H. Poelman, X. Ye, I.F.J. Vankelecom, P.A. Jacobs, D.E.De Vos, Au^0 nanocolloids as recyclable quasihomogeneous metal catalysts in the chemoselective hydrogenation of α,β-unsaturated aldehydes and ketones to allylic alcohols, Catal. Today 122 (2007) 352–360, https://doi.org/10.1016/j.cattod.2007.02.021.
[7] Y. Zhang, X. Cui, F. Shi, Y. Deng, Nano-gold catalysis in fine chemical synthesis, Chem. Rev. 112 (2012) 2467–2505, https://doi.org/10.1021/cr200260m.
[8] I.X. Green, W. Tang, M. Neurock, J.T. Yates, Dual perimeter sites, Acc. Chem. Res. 47 (2014) 805–815, https://doi.org/10.1021/ar400196f.
[9] B.K. Min, C.M. Friend, Heterogeneous gold-based catalysis for green chemistry: Low-temperature CO oxidation and propene oxidation, Chem. Rev. 107 (2007) 2709–2724, https://doi.org/10.1021/cr050954d.
[10] D.A. Panayotov, J.R. Morris, Surface chemistry of Au/TiO_2: thermally and photolytically activated reactions, Surf. Sci. Rep. 71 (2016) 77–271, https://doi.org/10.1016/j.surfrep.2016.01.002.
[11] W. Hou, S.B. Cronin, A review of surface plasmon resonance-enhanced photocatalysis, Adv. Funct. Mater. 23 (2013) 1612–1619, https://doi.org/10.1002/adfm.201202148.
[12] S. Bagheri, N. Muhd Julkapli, S. Bee Abd Hamid, Titanium dioxide as a catalyst support in heterogeneous catalysis, Sci. World J. (2014 () (2014), https://doi.org/10.1155/2014/727496.
[13] I.M. Arabatzis, T. Stergiopoulos, D. Andreeva, S. Kitova, S.G. Neophytides, P. Falaras, Characterization and photocatalytic activity of Au/TiO_2 thin films for azo-dye degradation, J. Catal. 220 (2003) 127–135, https://doi.org/10.1016/S0021-9517(03)00241-0.
[14] E.V. Rebrov, A. Berenguer-Murcia, B.F.G. Johnson, J.C. Schouten, Gold supported on mesoporous titania thin films for application in microstructured reactors in low-temperature water-gas shift reaction, Catal. Today 138 (2008) 210–215, https://doi.org/10.1016/j.cattod.2008.06.029.
[15] M. Crişan, D. Mardare, A. Ianculescu, N. Drăgan, I. Niţoi, D. Crişan, M. Voicescu, L. Todan, P. Oancea, C. Adomniţei, M. Dobromir, M. Gabrovska, B. Vasile, Iron doped TiO_2 films and their photoactivity in nitrobenzene removal from water, Appl. Surf. Sci. 455 (2018) 201–215, https://doi.org/10.1016/j.apsusc.2018.05.124.
[16] W. Tu, Y. Zhou, Z. Zou, Photocatalytic conversion of CO_2 into renewable hydrocarbon fuels: state-of-the-art accomplishment, challenges, and prospects, Adv. Mater. 26 (2014) 4607–4626, https://doi.org/10.1002/adma.201400087.
[17] X. Zhang, X. Li, D. Zhang, N.Q. Su, W. Yang, H.O. Everitt, J. Liu, Product selectivity in plasmonic photocatalysis for carbon dioxide hydrogenation, Nat. Commun. 8 (2017) 1–9, https://doi.org/10.1038/ncomms14542.
[18] T. Oshikiri, K. Ueno, H. Misawa, Plasmon-induced ammonia synthesis through nitrogen photofixation with visible light irradiation, Angew. Chem. 126 (2014) 9960–9963, https://doi.org/10.1002/ange.201404748.
[19] X.Y. Liu, A. Wang, T. Zhang, C.Y. Mou, Catalysis by gold: new insights into the support effect, Nano Today 8 (2013) 403–416, https://doi.org/10.1016/j.nantod.2013.07.005.
[20] A. Corma, H. Garci, Supported gold nanoparticles as catalysts for organic reactions, Chem. Soc. Rev. 37 (2008) 2096–2126, https://doi.org/10.1039/b707314n.
[21] M. Haruta, S. Tsubota, T. Kobayashi, H. Kageyama, M.J. Genet, B. Delmon, Low-temperature oxidation of CO over gold supported on TiO_2, α-Fe_2O_3, and Co_3O_4, J. Catal. 144 (1993) 175–192, https://doi.org/10.1006/jcat.1993.1322.
[22] M. Sankar, Q. He, R.V. Engel, M.A. Sainna, A.J. Logsdail, A. Roldan, D.J. Willock, N. Agarwal, C.J. Kiely, G.J. Hutchings, Role of the Support in Gold-Containing Nanoparticles as Heterogeneous Catalysts, Chem. Rev. 120 (2020) 3890–3938, https://doi.org/10.1021/acs.chemrev.9b00662.
[23] F. Moreau, G.C. Bond, Influence of the surface area of the support on the activity of gold catalysts for CO oxidation, Catal. Today 122 (2007) 215–221, https://doi.org/10.1016/j.cattod.2006.12.001.
[24] E.V. Rebrov, A. Berenguer-Murcia, H.E. Skelton, B.F.G. Johnson, A.E.H. Wheatley, J.C. Schouten, Capillary microreactors wall-coated with mesoporous titania thin film catalyst supports, Lab Chip 9 (2009) 503–506, https://doi.org/10.1039/b815716b.
[25] Z.R. Ismagilov, E.V. Matus, A.M. Yakutova, L.N. Protasova, I.Z. Ismagilov, M. A. Kerzhentsev, E.V. Rebrov, J.C. Schouten, Design of Pt-Sn catalysts on mesoporous titania films for microreactor application, Catal. Today 147 (2009) 81–86, https://doi.org/10.1016/j.cattod.2009.07.046.
[26] E.V. Rebrov, J.C. Schouten, Limiting withdrawal rate and maximum film thickness during dip-coating of titania sols onto a Si substrate, Chem. Eng. Process. Process. Intensif. 50 (2011) 1063–1068, https://doi.org/10.1016/j.cep.2011.05.025.
[27] L.N. Protasova, E.V. Rebrov, T.S. Glazneva, A. Berenguer-Murcia, Z.R. Ismagilov, J. C. Schouten, Control of the thickness of mesoporous titania films for application in multiphase catalytic microreactors, J. Catal. 271 (2010) 161–169, https://doi.org/10.1016/j.jcat.2009.07.013.
[28] N. Cherkasov, A.O. Ibhadon, E.V. Rebrov, Novel synthesis of thick wall coatings of titania supported Bi poisoned Pd catalysts and application in selective hydrogenation of acetylene alcohols in capillary microreactors, Lab Chip 15 (2015) 1952–1960, https://doi.org/10.1039/c4lc01066c.
[29] S.D. Svetlov, D.A. Sladkovskiy, K.V. Semikin, A.V. Utemov, R.S. Abiev, E. V. Rebrov, Synthesis of thin titania coatings onto the inner surface of quartz tubes and their photoactivity in decomposition of methylene blue and rhodamine b, Catalysts 11 (2021), https://doi.org/10.3390/catal11121538.
[30] N. Pradhan, A. Pal, T. Pal, Silver nanoparticle catalyzed reduction of aromatic nitro compounds, Colloids Surf. A Physicochem. Eng. Asp. 196 (2002) 247–257, https://doi.org/10.1016/S0927-7757(01)01040-8.
[31] K. Esumi, K. Miyamoto, T. Yoshimura, Comparison of PAMAM-Au and PPI-Au nanocomposites and their catalytic activity for reduction of 4-nitrophenol, J. Colloid Interface Sci. 254 (2002) 402–405, https://doi.org/10.1006/jcis.2002.8580.
[32] S. Wunder, Y. Lu, M. Albrecht, M. Ballauff, Catalytic activity of faceted gold nanoparticles studied by a model reaction: Evidence for substrate-induced surface restructuring, ACS Catal. 1 (2011) 908–916, https://doi.org/10.1021/cs200208a.
[33] N.R. Jana, L. Gearheart, C.J. Murphy, Wet chemical synthesis of high aspect ratio cylindrical gold nanorods, J. Phys. Chem. B 105 (2001) 4065–4067, https://doi.org/10.1021/jp0107964.
[34] O.V. Kalashnikova, I.N. Sokolik, Modeling the radiative properties of nonspherical soil-derived mineral aerosols, J. Quant. Spectrosc. Radiat. Transf. 87 (2004) 137–166, https://doi.org/10.1016/j.jqsrt.2003.12.026.
[35] J. Andrieux, U.B. Demirci, P. Miele, Langmuir-Hinshelwood kinetic model to capture the cobalt nanoparticles-catalyzed hydrolysis of sodium borohydride over a wide temperature range, Catal. Today 170 (2011) 13–19, https://doi.org/10.1016/j.cattod.2011.01.019.
[36] K. Vasanth Kumar, K. Porkodi, A. Selvaganapathi, Constrain in solving Langmuir-Hinshelwood kinetic expression for the photocatalytic degradation of Auramine O aqueous solutions by ZnO catalyst, Dye. Pigment. 75 (2007) 246–249, https://doi.org/10.1016/j.dyepig.2006.05.035.
[37] A. Guinier, G. Fournet, Small-Angle Scattering of X-Rays, John Wiley & Sons, Inc, New York, 1955.
[38] S. Pabisch, B. Feichtenschlager, G. Kickelbick, H. Peterlik, Effect of interparticle interactions on size determination of zirconia and silica based systems - A comparison of SAXS, DLS, BET, XRD and TEM, Chem. Phys. Lett. 521 (2012) 91–97, https://doi.org/10.1016/j.cplett.2011.11.049.
[39] M. Benkovicova, K. Vegso, P. Siffalovic, M. Jergel, S. Luby, E. Majkova, Preparation of gold nanoparticles for plasmonic applications, Thin Solid Films 543 (2013) 138–141, https://doi.org/10.1016/j.tsf.2013.01.048.

[40] D. Geißler, C. Gollwitzer, A. Sikora, C. Minelli, M. Krumrey, U. Resch-Genger, Effect of fluorescent staining on size measurements of polymeric nanoparticles using DLS and SAXS, Anal. Methods 7 (2015) 9785–9790, https://doi.org/10.1039/c5ay02005k.
[41] U. Kreibig, M. Vollmer, Optical Properties of Metal Clusters, Springer, US, New York, 1995.
[42] B. Palpant, B. Prével, Optical properties of gold clusters in the size range 2–4 nm, Phys. Rev. B - Condens. Matter Mater. Phys. 57 (1998) 1963–1970, https://doi.org/10.1103/PhysRevB.57.1963.
[43] P.K. Jain, K.S. Lee, I.H. El-Sayed, M.A. El-Sayed, Calculated absorption and scattering properties of gold nanoparticles of different size, shape, and composition: applications in biological imaging and biomedicine, J. Phys. Chem. B 110 (2006) 7238–7248, https://doi.org/10.1021/jp057170o.
[44] H. Hövel, S. Fritz, A. Hilger, U. Kreibig, M. Vollmer, Width of cluster plasmon resonances: bulk dielectric functions and chemical interface damping, Phys. Rev. B 48 (1993) 18178–18188, https://doi.org/10.1103/PhysRevB.48.18178.
[45] T.J. Norman, C.D. Grant, D. Magana, J.Z. Zhang, J. Liu, D. Cao, F. Bridges, A. Van Buuren, Near, Infrared Opt. Absorpt. Gold. Nanopart. Aggreg., J. Phys. Chem. B 106 (2002) 7005–7012, https://doi.org/10.1021/jp0204197CCC:22.00.
[46] V. Amendola, M. Meneghetti, Size evaluation of gold nanoparticles by UV–vis, Spectrosc., J. Phys. Chem. C. 113 (2009) 4277–4285, https://doi.org/10.1021/jp8082425.
[47] R. Fenger, E. Fertitta, H. Kirmse, A.F. Thünemann, K. Rademann, Size dependent catalysis with CTAB-stabilized gold nanoparticles, Phys. Chem. Chem. Phys. 14 (2012) 9343–9349, https://doi.org/10.1039/c2cp40792b.
[48] B.G. Donoeva, D.S. Ovoshchnikov, V.B. Golovko, Establishing a Au nanoparticle size effect in the oxidation of cyclohexene using gradually changing Au catalysts, ACS Catal. 3 (2013) 2986–2991, https://doi.org/10.1021/cs400701j.
[49] D. Buso, G. Busato, M. Guglielmi, A. Martucci, V. Bello, G. Mattei, P. Mazzoldi, M. L. Post, Selective optical detection of H_2 and CO with SiO_2 sol-gel films containing NiO and Au nanoparticles, Nanotechnology 18 (2007), https://doi.org/10.1088/0957-4484/18/47/475505.
[50] W. Haiss, N.T.K. Thanh, J. Aveyard, D.G. Fernig, Determination of size and concentration of gold nanoparticles from UV-Vis spectra, Anal. Chem. 79 (2007) 4215–4221, https://doi.org/10.1021/ac0702084.
[51] T. van der Meulen, A. Mattson, L. Österlund, A comparative study of the photocatalytic oxidation of propane on anatase, rutile, and mixed-phase anatase-rutile TiO_2 nanoparticles: Role of surface intermediates, J. Catal. 251 (2007) 131–144, https://doi.org/10.1016/j.jcat.2007.07.002.
[52] J. Zhang, P. Zhou, J. Liu, J. Yu, New understanding of the difference of photocatalytic activity among anatase, rutile and brookite TiO_2, Phys. Chem. Chem. Phys. 16 (2014) 20382–20386, https://doi.org/10.1039/c4cp02201g.
[53] D.A.H. Hanaor, C.C. Sorrell, Review of the anatase to rutile phase transformation, J. Mater. Sci. 46 (2011) 855–874, https://doi.org/10.1007/s10853-010-5113-0.
[54] R. Reichert, Z. Jusys, R.J. Behm, Au/TiO_2 Photo(electro)catalysis: the role of the au cocatalyst in photoelectrochemical water splitting and photocatalytic, H_2 Evol., J. Phys. Chem. C. 119 (2015) 24750–24759, https://doi.org/10.1021/acs.jpcc.5b08428.
[55] Y. Kim, J.G. Smith, P.K. Jain, Harvesting multiple electron-hole pairs generated through plasmonic excitation of Au nanoparticles, Nat. Chem. 10 (2018) 763–769, https://doi.org/10.1038/s41557-018-0054-3.
[56] M. Hajfathalian, K.D. Gilroy, A. Yaghoubzade, A. Sundar, T. Tan, R.A. Hughes, S. Neretina, Photocatalytic enhancements to the reduction of 4-nitrophenol by resonantly excited triangular gold-copper nanostructures, J. Phys. Chem. C. 119 (2015) 17308–17315, https://doi.org/10.1021/acs.jpcc.5b04618.
[57] N.K.R. Bogireddy, U. Pal, L.M. Gomez, V. Agarwal, Size controlled green synthesis of gold nanoparticles using Coffea arabica seed extract and their catalytic performance in 4-nitrophenol reduction, RSC Adv. 8 (2018) 24819–24826, https://doi.org/10.1039/c8ra04332a.
[58] R. Seoudi, F.A. Al-Marhaby, Synthesis, characterization and photocatalytic application of different sizes of gold nanoparticles on 4-nitrophenol, World J. Nano Sci. Eng. 06 (2016) 120–128, https://doi.org/10.4236/wjnse.2016.63012.
[59] L. Sun, M. Zhou, Z. Yin, L. Zhang, B. Dou, W. Su, Rapid synthesis of gold nanoparticles for photocatalytic reduction of 4-nitrophenol, Res. Chem. Intermed. 46 (2020) 5117–5131, https://doi.org/10.1007/s11164-020-04254-0.